

P2-K_{0.75}[Ni_{1/3}Mn_{2/3}]O₂ Cathode Material for High Power and Long Life Potassium-Ion Batteries

Jae Hyeon Jo, Ji Ung Choi, Yun Ji Park, Young Hwa Jung, Docheon Ahn, Tae-Yeol Jeon, Hyungsub Kim, Jongsoon Kim,* and Seung-Taek Myung*

Rationally designed P2-K_{0.75}[Ni_{1/3}Mn_{2/3}]O₂ is introduced as a novel cathode material for potassium-ion batteries (KIBs). P2-K_{0.75}[Ni_{1/3}Mn_{2/3}]O₂ cathode material designed through electrochemical ion-exchange from P2-Na_{2/3}[Ni_{1/3}Mn_{2/3}]O₂ exhibits satisfactory electrode performances; 110 mAh g⁻¹ (20 mA g⁻¹) retaining 86% of capacity for 300 cycles and unexpectedly high reversible capacity of about 91 mAh g⁻¹ (1400 mA g⁻¹) with excellent capacity retention of 83% over 500 cycles. According to theoretical and experimental investigations, the overall potassium storage mechanism of P2-K_{0.75}[Ni_{1/3}Mn_{2/3}]O₂ is revealed to be a single-phase reaction with small lattice change upon charge and discharge, presenting the Ni^{4+/2+} redox couple reaction. Such high power capability is possible through the facile K⁺ migration in the K_{0.75}[Ni_{1/3}Mn_{2/3}]O₂ structure with a low activation barrier energy of ≈210 meV. These findings indicate that P2-K_{0.75}[Ni_{1/3}Mn_{2/3}]O₂ is a promising candidate cathode material for high-rate and long-life KIBs.

system are very rational to follow the footsteps that have accomplished in LIBs. Recently, potassium-ion batteries (KIBs) have begun to attract significant attention as promising alternatives to LIBs owing to their similar chemistries and the high operation voltage; namely, standard redox potential of -2.94 V versus standard hydrogen electrode (SHE) for K⁺/K and -3.04 V versus SHE for Li⁺/Li.^[5-7] Potassium exhibits the smallest Stokes radius and the weakest Lewis acidity, affecting fast ionic conductivity in the electrolyte. Graphite is the common anode for hosting the lithium ions in LIBs. From this point of view, it is notable that potassium ions are inserted into graphite to form KC₈, while there is thermodynamical unfavorability for intercalation sodium ions into graphite. Therefore, the chemistry of KIBs

are far closer to that of LIBs, so that searching of appropriate cathode materials is an important step to realization of KIBs that can compete with LIBs in near future^[8-14]

Recently, various intercalation cathode materials have been investigated as cathode candidates for KIB, including layered compounds, olivine compounds, Prussian blue analogues, and organic polycyclic compounds. Some examples include P2-type K_xMeO₂ (Me = transition metal),^[15-20] P3-type K_xMeO₂ (Me = transition metal),^[12,17-30] P'2-type K_{0.3}MnO₂,^[31] K₃V₂(PO₄)₃,^[32] KMeP₂O₇ (Me = Ti, V, and Mo),^[33] K₂V₃O₈,^[34] Prussian blue analogues,^[8,35-39] and 3, 4, 9, 10-perylenetetracarboxylic acid dianhydride (PTCDA)^[40] and poly anthraquinonyl sulfide (PAQS).^[41] Amongst these materials, the layered-type cathode materials have been most extensively investigated because of their relatively large interlayer distance and diffusion paths, which can sufficiently accommodate large K⁺ ions (1.37 Å). Although some earlier works have demonstrated the reversible insertion/extraction of K⁺ ions, improved cycling stability and rate capability are needed for battery applications. To satisfy the above concerns, cathode materials should be able to accommodate the large K⁺ ions into their structure for long term. Improvement of the rate capability is necessary through a rational design of cathode materials composed of cost-effective elements.

One of the interesting approaches is electrochemical ion-exchange of sodiated transition metal oxides in potassium cells, which enables exploration of new compounds. Sada et al.,^[42] introduced that P2-Na_{0.84}CoO₂ was first charged for desodiation

1. Introduction

Lithium-ion batteries (LIBs) have drawn significant attention for rechargeable energy storage for portable electronic devices and electric vehicles (EVs) because of their high energy densities and excellent rate capabilities.^[1-4] Many recent works have pursued to further increase energy densities of LIBs; however, it seems to be difficult to overcome the theoretical limits using existing chemistries and materials. This triggers exploration of beyond LIBs that can substantially alter the energy storage systems. For this reason, the approaches toward sodium and potassium

J. H. Jo, J. U. Choi, Y. J. Park, Prof. J. Kim, Prof. S.-T. Myung
Department of Nanotechnology and Advanced Materials Engineering
& Sejong Battery Institute
Sejong University
Seoul 05006, South Korea
E-mail: jongsoonkim@sejong.ac.kr; smyung@sejong.ac.kr

Dr. Y. H. Jung, Dr. D. Ahn, Dr. T.-Y. Jeon
Pohang Accelerator Laboratory
80 Jigokro-127-beongil, Nam-gu, Pohang, Gyeongbuk
Seoul 37673, South Korea

Dr. H. Kim
Korea Atomic Energy Research Institute
Daedeok-daero 989 Beon-Gil, Yuseong-gu, Daejeon 34507, South Korea

The ORCID identification number(s) for the author(s) of this article can be found under <https://doi.org/10.1002/aenm.201903605>.

DOI: 10.1002/aenm.201903605

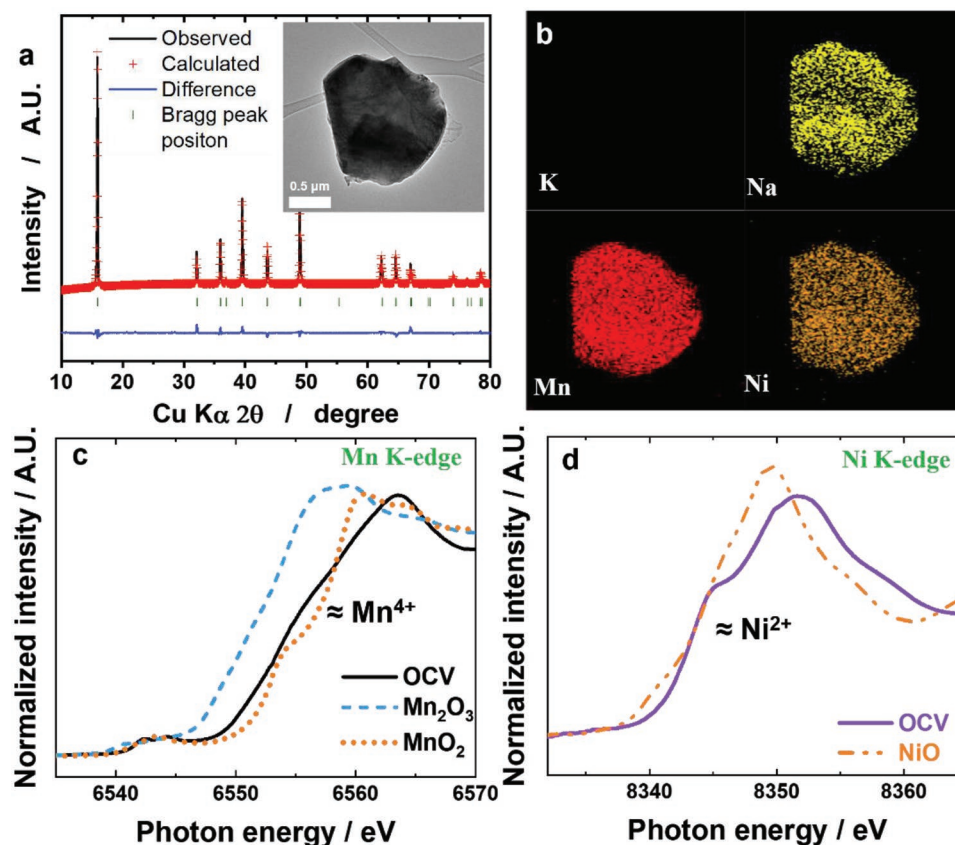


Figure 1. a) Rietveld refinement of XRD data for P2-Na_{2/3}[Ni_{1/3}Mn_{2/3}]O₂ (inset: TEM image of P2-Na_{2/3}[Ni_{1/3}Mn_{2/3}]O₂) and b) the corresponding EDS mapping images of inset TEM image shown in (a); XANES spectra of c) Mn K-edge and d) Ni K-edge for P2-Na_{2/3}[Ni_{1/3}Mn_{2/3}]O₂.

in K-based electrolytes, which yielded a new P2-K_{0.5}CoO₂ compound. Hwang et al.,^[22] used a similar approach to produce P3-K_xCrO₂ from O3-NaCrO₂. These works indicate that sodiated transition metal oxides can be potassiated via electrochemical ion-exchange in potassium (K) cells, in which the released Na⁺ do not interrupt the K⁺ de/intercalation.

So far as we know, a synthetic process for such a P2 structure has not yet been established, because the large ionic size of K⁺ results in crystallization into the P3 structure being favored. Also, many-layered cathode materials do not show a high operation voltage.^[12–28] Provided that synthesis of P2-K_x[Ni_{1/3}Mn_{2/3}]O₂ is possible, this would enable the realization of a high-energy-density cathode for KIBs. These issues motivated us to overcome the synthetic difficulties associated with P2-K_x[Ni_{1/3}Mn_{2/3}]O₂ by adopting electrochemical ion-exchange of P2-Na_{2/3}[Ni_{1/3}Mn_{2/3}]O₂ in K cells. Herein, we introduce a layered Ni- and Mn-based P2-K_x[Ni_{1/3}Mn_{2/3}]O₂ cathode material that can accommodate repeated insertion/extraction of large K⁺ ions without sacrificing the structural stability. P2-K_{0.75}[Ni_{1/3}Mn_{2/3}]O₂ was prepared via the electrochemical ion-exchange of P2-Na_{2/3}[Ni_{1/3}Mn_{2/3}]O₂ for use as a high-performance cathode for KIBs. Notably, the proposed P2-K_{0.75}[Ni_{1/3}Mn_{2/3}]O₂ cathode delivers a high reversible capacity of 110 mA h g⁻¹ at a current of 20 mA g⁻¹ with outstanding cycling stability (> 86% capacity retention) for 300 cycles in K cells. Further, P2-K_{0.75}[Ni_{1/3}Mn_{2/3}]O₂ exhibits

a high rate cyclability with capacity retention of 83% for 500 cycles when tested at a current of 1400 mA g⁻¹. Operando synchrotron X-ray diffraction (o-SXRD) and X-ray absorption near-edge structure (XANES) spectroscopic investigations demonstrate that the P2-K_{0.75}[Ni_{1/3}Mn_{2/3}]O₂ undergoes a simple single-phase reaction, in which the corresponding electrochemical activity is associated with the Ni^{4+/2+} redox pair. Through combined studies using first-principles calculation and various experiments, we report the promising potassium storage ability of layered P2-K_{0.75}[Ni_{1/3}Mn_{2/3}]O₂ and unveil the electrochemical reaction mechanism for the excellent reversible behavior of the K⁺ de/intercalation reaction as a cathode material for KIBs.

2. Results and Discussion

2.1. Preparation of P2-K_{0.75}[Ni_{1/3}Mn_{2/3}]O₂

P2-Na_{2/3}[Ni_{1/3}Mn_{2/3}]O₂ was synthesized via a spray pyrolysis method, and the crystal structure was analyzed by Rietveld refinement of XRD data assuming the rhombohedral *P*6₃/*m**mc* space group (Figure 1a and Table S1, Supporting Information). The observed pattern matched well with the calculated one without impurities. The calculated lattice parameters were *a* = 2.884(2) Å and *c* = 11.133(2) Å, which are consistent with the values in literature.^[43,44] The obtained particle was flat

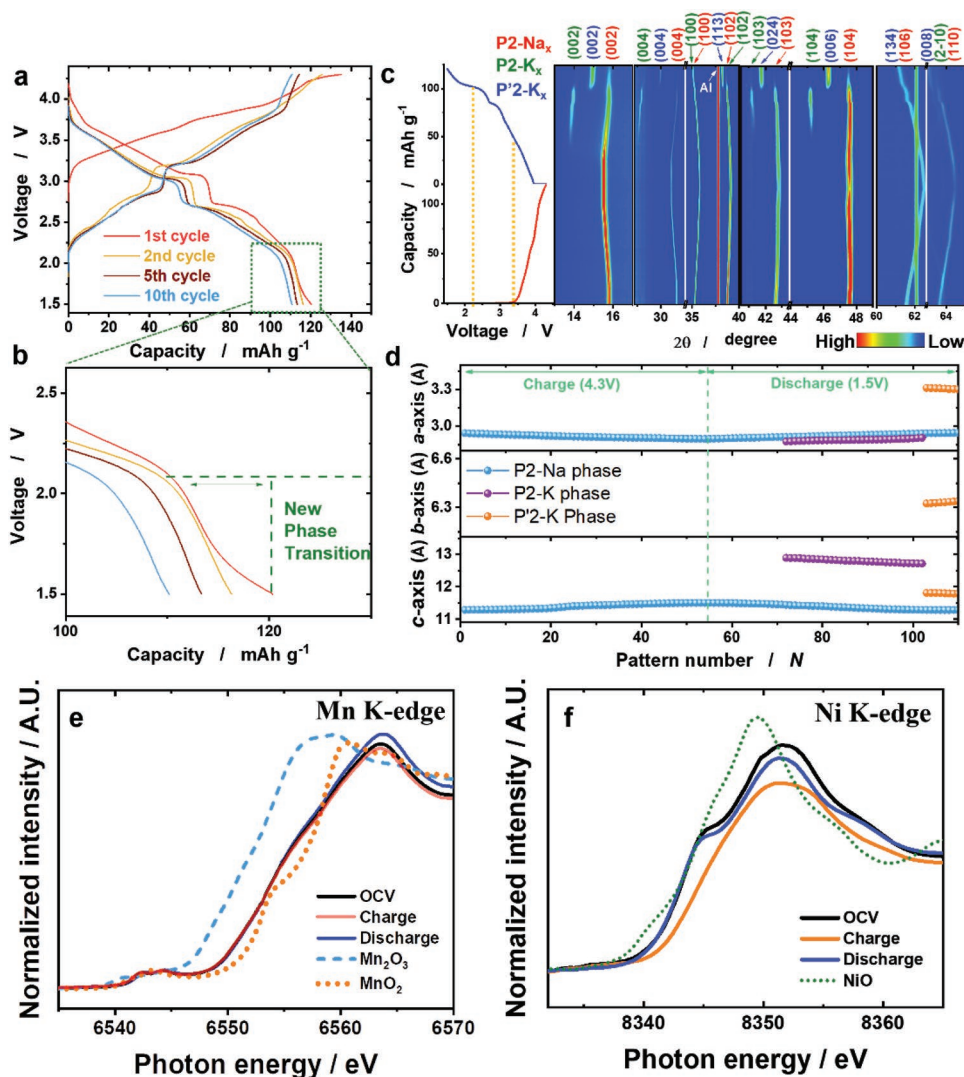


Figure 2. Electrochemical ion-exchange process: a) the charge–discharge curves for 1st, 2nd, 5th, and 10th cycle of K metal|0.5 M KPF₆ in EC:DEC = 1:1 (v/v)|P2-Na_{2/3}[Ni_{1/3}Mn_{2/3}]O₂ cell tested at 20 mA g⁻¹; b) magnified charge–discharge curve of for 1st, 2nd, 5th, and 10th cycle; c) operando SXRD results for P2-Na_{2/3}[Ni_{1/3}Mn_{2/3}]O₂ cell during the first cycle and the corresponding variation in lattice parameters; d) the corresponding calculated lattice parameters for *o*-SXRD pattern; e) XANES results of Mn K-edge and f) XANES results of Ni K-edge for the fresh, desodiated Na_{0.16}[Ni_{1/3}Mn_{2/3}]O₂ charged to 4.3 V, and potassiated K_{0.49}Na_{0.16}[Ni_{1/3}Mn_{2/3}]O₂ discharged to 1.5 V.

with an estimated size of about 2 μm , and Na, Mn, and Ni were homogeneous distributed in the particles (Figure 1b) The XANES spectra of the Mn and Ni K-edges for the as-synthesized P2-Na_{2/3}[Ni_{1/3}Mn_{2/3}]O₂ indicate that the oxidation state of Mn was close to 4+ (Figure 1c), whereas the Ni had a photon energy similar to that of Ni²⁺O (Figure 1d).

The electrochemical Na⁺/K⁺ ion-exchange was performed in K cells configured with P2-Na_{2/3}[Ni_{1/3}Mn_{2/3}]O₂ | 0.5 M KPF₆ in EC:DEC (1:1 v/v %) | K metal between 1.5 and 4.3 V at 20 mA g⁻¹ for 10 cycles (Figure 2a). At the first charge (desodiation), the extracted Na content was 0.51 mol (133 mAh g⁻¹) from the P2-Na_{2/3}[Ni_{1/3}Mn_{2/3}]O₂ electrode, giving Na_{0.16}[Ni_{1/3}Mn_{2/3}]O₂. The presence of long plateaus above 4.1 V versus Na⁺/Na, attributed to the P2–O2 phase transition, is typical in P2-Na_{2/3}[Ni_{1/3}Mn_{2/3}]O₂ (Figure S1, Supporting Information), whereas the phase transition is not evident at the first

charge. In addition, the obtained charge capacity in the K cell was lower than that for testing in Na cells (generally, ≈ 170 mAh g⁻¹).^[44] The operation voltage observed in the K cells was lower and steeper than that observed in Na cells, which may be attributed to the intercalation of different ionic species, as the shapes of the first and second charge curves differed. The first charge curve consisted of a smooth increase profile and is related to the extraction of Na⁺ upon oxidation. By contrast, for the second charge, there are several voltage plateaus involved with deintercalation of K⁺ during the charge to 4.3 V. The cation/vacancy ordering is more evident for the depotassiation relative to the sodiation. During the subsequent discharge process (potassiation) to 1.5 V, the K⁺ ions were progressively intercalated with several voltage steps, and the corresponding capacity reached a discharge capacity of 120 mAh g⁻¹ at the first cycle. A similar discharge curve profile was observed for the second cycle

despite the appearance of a tail at the end of the first cycle (Figure 2b). After the second cycle, the subsequent charge and discharge profiles were almost identical to the curves observed at the 10th cycle, with abrupt voltage decay at the end of discharge. Because of the tail appearing at the first discharge, we compared the o-SXRD patterns after discharge for the 1st, 2nd, 5th, and 10th cycle. Figure 2c presents contour maps of o-SXRD patterns for P2-Na_{2/3}[Ni_{1/3}Mn_{2/3}]O₂ measured at the first charge (desodiation) and discharge (potassiation) in a K cell. During the charge (desodiation) to 4.3 V, a monotonous shift of the (002) and (004) peaks toward lower angle was observed, whereas the (100), (102), (103), (104), (106), and (110) peaks moved to higher angle to Na_{0.16}[Ni_{1/3}Mn_{2/3}]O₂ in the o-SXRD patterns. No other new peaks appeared during the charge process. The calculated lattice parameters also showed slight variations in both the *a*- and *c*-axes during desodiation, suggesting the occurrence of a single-phase reaction. As mentioned in Figure 2a, it is common for P2-Na_{2/3}[Ni_{1/3}Mn_{2/3}]O₂ to undergo a phase transition from P2 to O2; however, this phase transition was not evident, and the original layer structure was maintained during the desodiation process. On discharge (potassiation), all the diffraction peaks of P2-Na_{2/3}[Ni_{1/3}Mn_{2/3}]O₂ returned to their original peak positions. Unexpectedly, new peaks appeared at 14°, 28.3°, 41.8°, 45.3°, and 63.8° (2θ) in the voltage range of 3.5–2.1 V, which can be indexed as (002), (004), (103), (104), and (2–10) peaks, respectively, for the potassiated P2-K_xNa_{0.16}[Ni_{0.3}Mn_{0.7}]O₂ (*x* ≤ 0.44). Concurrently, the relative peak intensities belonging to (00*l*) planes decreased because of the formation of the new potassiated P2 phase. Further potassiation of the P2 structure showing a tail resulted in a phase transformation from P2 to P'2 (Figure S2, Supporting Information) below 2.1 V, with characteristic peaks of (002), (004), (103), and (104). The variations in the *a*- and *c*-axes parameters during the first cycle are summarized in Figure 2d. These variations in the lattice parameters indicate a considerable amount of K⁺ insertion into the desodiated host structure on discharge. To identify the valences of the transition metals during the first desodiation and potassiation, ex situ XANES measurements were performed (Figure 2e,f). The Mn K-edge spectrum of the fresh Na_{2/3}[Ni_{1/3}Mn_{2/3}]O₂ was located at similar energy as that of Mn⁴⁺O₂, indicating that the oxidation state of Mn in Na_{2/3}[Ni_{1/3}Mn_{2/3}]O₂ is 4+ (Figure 2e). Even after desodiation and potassiation, it is notable that there were no changes in the spectra, indicating that Mn was inactive in the compound. For the Ni K-edge spectrum (Figure 2f), the fresh Ni K-edge absorption was similar to that of Ni²⁺O. However, on desodiation, the Ni K-edge absorption shifted to higher energy because of oxidation of Ni²⁺ toward Ni⁴⁺, which was reversible on potassiation showing a reduction from Ni⁴⁺ to Ni²⁺. This finding suggests that the Ni^{4+/2+} redox pair is responsible for the activity during potassiation.

To further confirm the phase formation at the end of discharge (1.5 V), XRD analysis of the cycled electrodes was performed (Figure 3a). Compared to the fresh P2-Na_{2/3}[Ni_{1/3}Mn_{2/3}]O₂, the new peak at 2θ = 15° and small peak at 2θ = 14° belong to potassiated orthorhombic P'2- and layered P2 phases, respectively, after the first discharge (Figure 3a-2). After the second cycle, the P2-phase originated from P2-Na_{2/3}[Ni_{1/3}Mn_{2/3}]O₂ and the new P'2-K_x[Ni_{1/3}Mn_{2/3}]O₂ were negligible (Figure 3a-3). This tendency became more evident as cycling progressed (Figure 3a-4 to 6),

and the sodium-free P2-K_{0.75}[Ni_{1/3}Mn_{2/3}]O₂ phase, determined by ICP-AES, was formed after the 10th cycle (Figure 3a-6).

To predict the possibility of K⁺ intercalation and diffusion pathways in the structure, we performed structural analyses using the bond-valence-sum energy landscape (BVLE) method using the Bond_Str program in the FullProf package. As shown in Figure 3b, the presence of vacant atomic sites for K⁺ ions between infinite layers composed of [Ni, Mn]O₆ octahedra along the *ab* plane and their atomic positions were verified. The predicted atomic position and Wyckoff position on K⁺ ions in the structure were (0, 0, 0.25) 2b and (0.67, 0.33, 0.25) 2d, respectively. Using Rietveld refinement of XRD data based on the predicted results of the BVLE analyses, we verified the detailed structural information for the electrochemically ionic exchanged K_{0.75}[Ni_{1/3}Mn_{2/3}]O₂ electrode (Figure 3c).

The structural refinement results of K_{0.75}[Ni_{1/3}Mn_{2/3}]O₂ showed good agreement with the P2 layer structure with *P6₃/mmc* space group without impurities and sodiated phases. The calculated lattice parameters for K_{0.75}[Ni_{1/3}Mn_{2/3}]O₂ were *a* = 2.906(2) Å and *c* = 12.603(5) Å, as shown in Table S3 (Supporting Information); these values are larger than those of the parent Na_{0.67}[Ni_{1/3}Mn_{2/3}]O₂, *a* = 2.884(2) Å and *c* = 11.133(2) Å. The K_{0.75}[Ni_{1/3}Mn_{2/3}]O₂ was observed using a transmission electron microscope (TEM) with energy dispersive spectroscopic (EDS) elemental mapping (Figure 3d,e). The particle shape was similar to that of Na_{2/3}[Ni_{1/3}Mn_{2/3}]O₂ (Figure 1b), and the corresponding selected-area electron diffraction (SAED) pattern along the [00-1] zone axis indicated the presence of a typical hexagonal layer structure (Figure 3d). The elemental mapping results (Figure 3e) revealed a homogeneous distribution of K, Ni, and Mn elements, whereas Na was not detectable in the mapping nor composition analytic data, which agrees with the ICP-AES results. Meanwhile, sodium was detected in the cycled glass-fiber separators used in the K cells, configured initially as K metal // 0.5 M KPF₆ in the ED:DEC // Na_{2/3}[Ni_{1/3}Mn_{2/3}]O₂ (Figure S3 and Table S4, Supporting Information). At the 10th cycle, the corresponding CE reached close to 100% (Figure 3f), as additional deintercalation by Na⁺ no longer occurred because of completion of the electrochemical Na⁺/K⁺ ion-exchange in K cells. The electrochemical ion-exchange process is summarized in Figure 4a,b. The starting Na_{2/3}[Ni_{1/3}Mn_{2/3}]O₂ had an interlayer distance of 5.5 Å, whereas the electrochemically formed P2-K_{0.75}[Ni_{1/3}Mn_{2/3}]O₂ had a larger interlayer distance (≈6.5 Å). This difference indicates that the large ionic size of K⁺ (1.38 Å) relative to that of Na⁺ (1.02 Å) is responsible for the enlargement of the interlayer distance.^[45]

Based on the structural information for P2-K_{0.75}[Ni_{1/3}Mn_{2/3}]O₂ confirmed through Rietveld refinement of XRD data, we performed first-principles calculation to predict the theoretical properties of P2-K_{0.75}[Ni_{1/3}Mn_{2/3}]O₂. As shown in Figure 5a, we prepared several K/vacancy configurations on various P2/O2-K_x[Ni_{1/3}Mn_{2/3}]O₂ (0 ≤ *x* ≤ 1) using cluster-assisted statistical mechanics (CASM) software and then calculated and arranged their formation energies. Based on the following equation, we predicted the redox potentials of P2/O2-K_x[Ni_{1/3}Mn_{2/3}]O₂ during de/potassiation

$$V = - \frac{E[\text{K}_{x_2}\text{Ni}_{1/3}\text{Mn}_{2/3}\text{O}_2] - E[\text{K}_{x_1}\text{Ni}_{1/3}\text{Mn}_{2/3}\text{O}_2] - (x_2 - x_1)E[\text{K}]}{(x_2 - x_1)F} \quad (1)$$

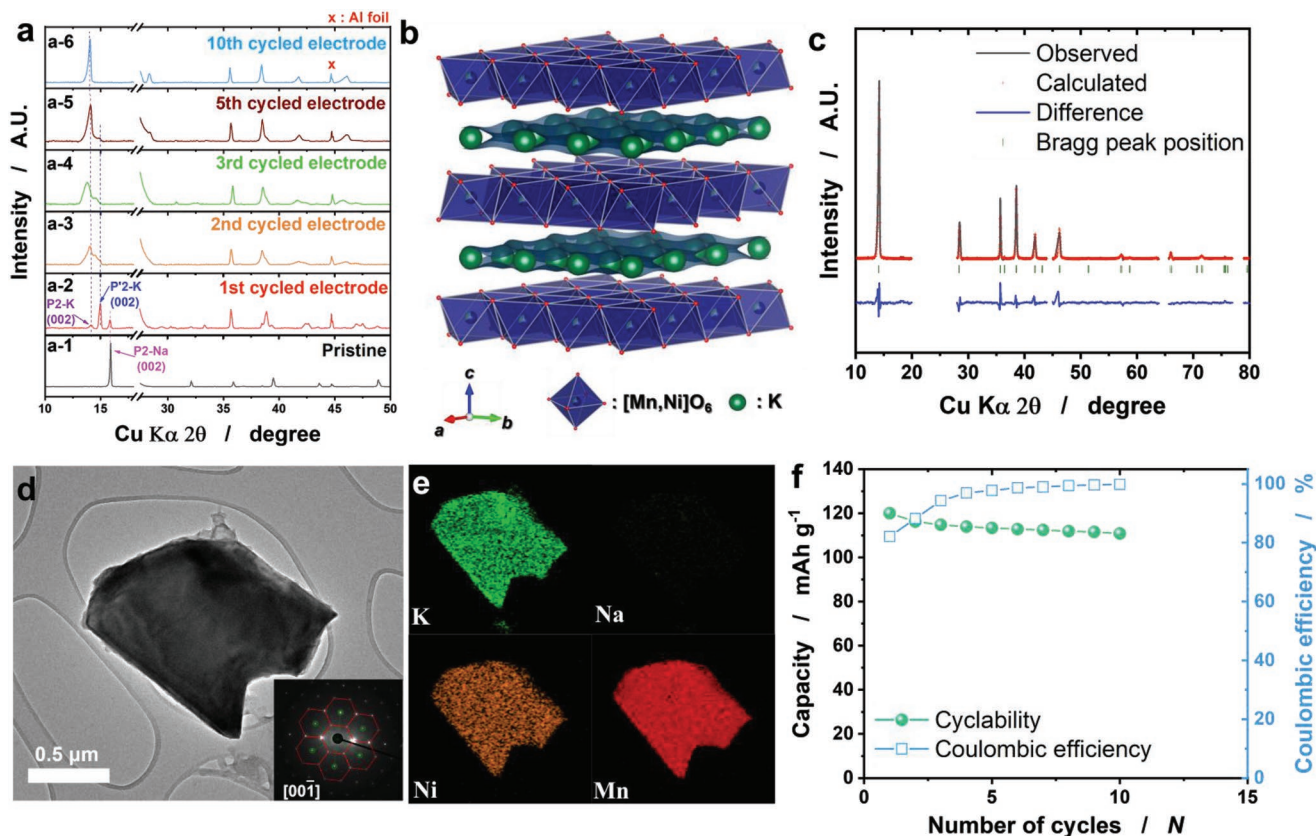


Figure 3. a) Ex situ XRD patterns of P2-Na_{2/3}[Ni_{1/3}Mn_{2/3}]O₂ in K cell (fresh, after 1st, 2nd, 3rd, 5th and 10th cycle); b) possible K⁺ sites in P2-K_{0.75}[Ni_{1/3}Mn_{2/3}]O₂ structure predicted through bond valence energy landscape (BVEL) analyses; c) Rietveld refinement of XRD data for the P2-K_{0.75}[Ni_{1/3}Mn_{2/3}]O₂ obtained after the electrochemical ion-exchange; d) TEM image of P2-K_{0.75}[Ni_{1/3}Mn_{2/3}]O₂ (inset: SAED pattern) and e) the resulting EDS mapping image shown in (d); f) Coulombic efficiency of P2-Na_{2/3}[Ni_{1/3}Mn_{2/3}]O₂ in K cell for electrochemical ion-exchange that was completed for 10 cycles.

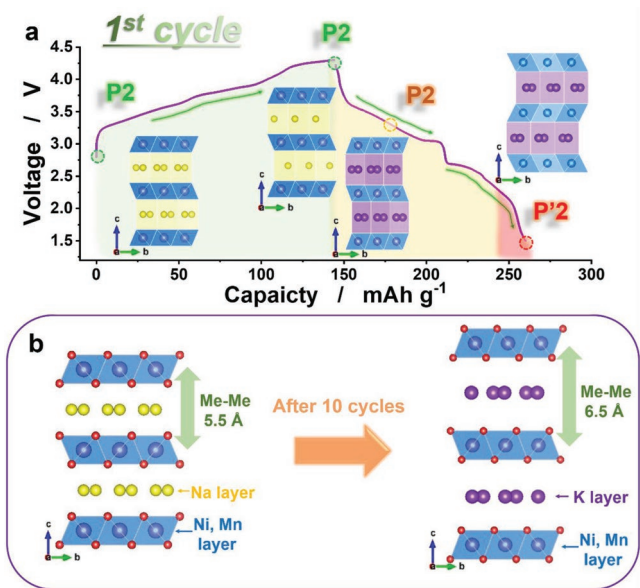


Figure 4. a) Electrochemical ion-exchange process of P2-Na_{2/3}[Ni_{1/3}Mn_{2/3}]O₂ during the first cycle; b) crystal structure models of P2-Na_{2/3}[Ni_{1/3}Mn_{2/3}]O₂ and P2-K_{0.75}[Ni_{1/3}Mn_{2/3}]O₂.

where V is the average redox potential of P2/O₂-K_x[Ni_{1/3}Mn_{2/3}]O₂ ($x_1 \leq x \leq x_2$) and $E[\text{K}_x\text{Ni}_{0.05}\text{Mn}_{0.95}\text{O}_2]$ represents the most stable formation energy of P2/O₂-K_x[Ni_{1/3}Mn_{2/3}]O₂. It was verified that P2-K_x[Ni_{1/3}Mn_{2/3}]O₂ phases are more stable than O2-K_x[Ni_{1/3}Mn_{2/3}]O₂ at the available operation voltage range between 1.5 and 4.3 V (vs K⁺/K) for KIBs. Figure 5b shows that the predicted redox potential of P2-K_x[Ni_{1/3}Mn_{2/3}]O₂ agrees well with the experimentally measured charge/discharge profile. It was also confirmed that in the voltage range of 1.5–4.3 V (vs K⁺/K), the P2-K_x[Ni_{1/3}Mn_{2/3}]O₂ can theoretically deliver a specific capacity of about 111 mAh g⁻¹, corresponding to de/intercalation of about 0.49 mol K per formula unit. The interesting point of P2-K_x[Ni_{1/3}Mn_{2/3}]O₂ during K⁺ de/intercalation is the P2–O₂ phase transition. It was predicted that the P2–O₂ phase transition of P2-K_x[Ni_{1/3}Mn_{2/3}]O₂ occurred when the K content in the structure was ≈ 0 or 1 mol (Figure 5a). As shown in Figure 5c, we arranged the predicted crystal structures for the most stable P2/O₂-K_x[Ni_{1/3}Mn_{2/3}]O₂ phases ($0 \leq x \leq 1$). It was predicted that the c -axis parameter was greatly decreased when the K content in the structure was close to ≈ 0 or ≈ 1 mol; in addition, decreasing the c -axis parameter of the prismatic-based (such as P2 or P3) layered-type structures resulted in oxygen sliding and a phase transition to octahedral-based (such as O2, O3, and OP4) layered-type structures.^[46] However, this large

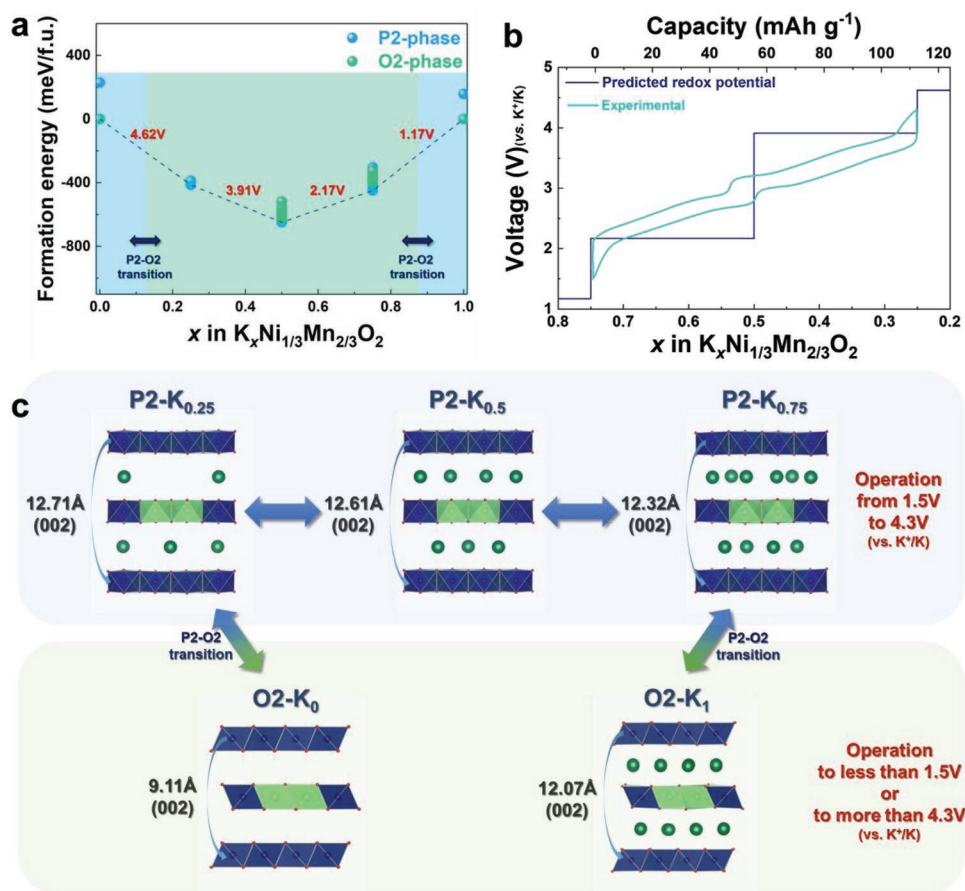


Figure 5. a) Formation energies of P2/O2-K_x[Ni_{1/3}Mn_{2/3}]O₂ with various K contents; b) comparison between experimentally measured charge/discharge curves and redox potentials predicted from first-principles calculations; c) predicted structural change of P2/O2-K_x[Ni_{1/3}Mn_{2/3}]O₂ as a function of K content.

structural change of the O2–P2 phase transition was accompanied by a large change in the formation energies, which resulted in too low redox potential between O2-K₀[Ni_{1/3}Mn_{2/3}]

O₂ and P2-K_{0.25}[Ni_{1/3}Mn_{2/3}]O₂ (≈1.17 V (vs K^{+/K})) and too high redox potential between P2-K_{0.75}[Ni_{1/3}Mn_{2/3}]O₂ and O2-K₁[Ni_{1/3}Mn_{2/3}]O₂ (≈4.62 V (vs K^{+/K})).

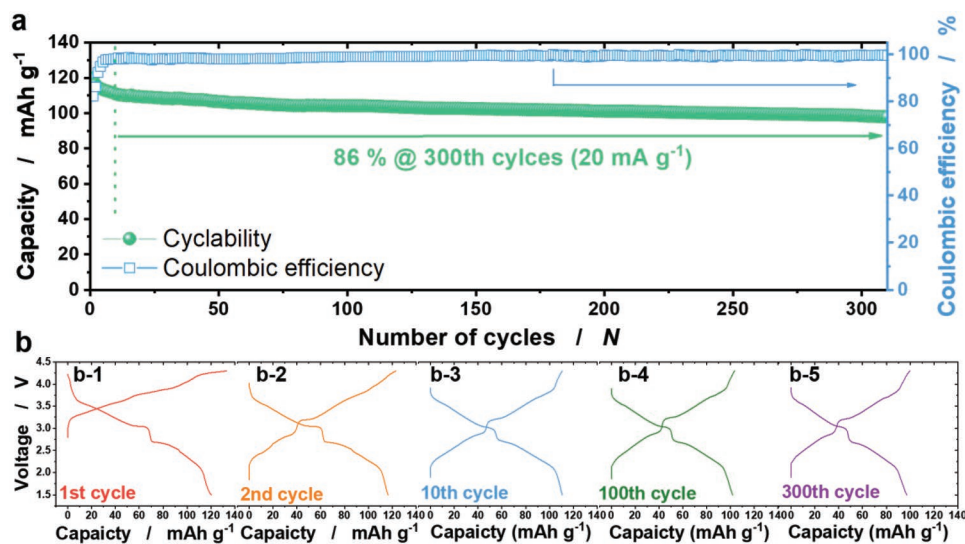


Figure 6. a) Long term cyclability of K metal|0.5 m KPF₆ in EC:DEC = 1:1 (v/v)|P2-K_{0.75}[Ni_{1/3}Mn_{2/3}]O₂ cell tested at 20 mA g⁻¹; b) selected charge-discharge voltage curves at 1st, 2nd, 10th, 100th, and 300th cycle at 20 mA g⁻¹.

After completion of the ion-exchange, the formed P2- $\text{K}_{0.75}[\text{Ni}_{1/3}\text{Mn}_{2/3}]\text{O}_2$ electrode delivered a high discharge capacity of 110 mAh g^{-1} (20 mA g^{-1}) at the 11th cycle and retained over 86% capacity retention for 300 cycles, with good CE over 99.5% (Figure 6a,b). It is notable that the $\text{K}_{0.75}[\text{Ni}_{1/3}\text{Mn}_{2/3}]\text{O}_2$ electrode exhibited an unexpectedly high discharge capacity of 91 mAh g^{-1} at 1400 mA g^{-1} , which is 85% of the discharge capacity tested at 20 mA g^{-1} (Figure 7a,b). A long-term cycling test at 1400 mA g^{-1} revealed that the $\text{K}_{0.75}[\text{Ni}_{1/3}\text{Mn}_{2/3}]\text{O}_2$ electrode was able to deliver $\approx 75 \text{ mAh g}^{-1}$ at the 500th cycle, thus retaining over 83% of the capacity for 500 cycles with a high CE ($>99.7\%$), as shown in Figure 7c,d.

The outstanding rate-capability of the $\text{K}_{0.75}[\text{Ni}_{1/3}\text{Mn}_{2/3}]\text{O}_2$ electrode was also confirmed using the nudged-elastic band

(NEB) method based on first-principles calculation. Indeed, there is appearance of K^+ /vacancy ordering when a low current was applied, while the ordering was less evident at high rates (Figures 6b and 7a). The difference in the capacity at 20 mA g^{-1} and 1.4 A g^{-1} was about 18 mAh g^{-1} (Figure 7a), which is a quite small difference observed in existing cathode materials for LIBs.^[16] Figure 7e shows the predicted K^+ diffusion motion between K1 and K2 sites in the structure, and the activation barrier energy required for the K^+ diffusion was only $\approx 210 \text{ meV}$, which is sufficiently low enough to ensure facile K^+ migration in the $\text{K}_{0.75}[\text{Ni}_{1/3}\text{Mn}_{2/3}]\text{O}_2$ structure. Furthermore, this value is highly similar to the activation barrier energies of conventional cathode materials for LIBs.^[47,48] From this consideration, it is thought that the smallest Stokes radius and the weakest Lewis

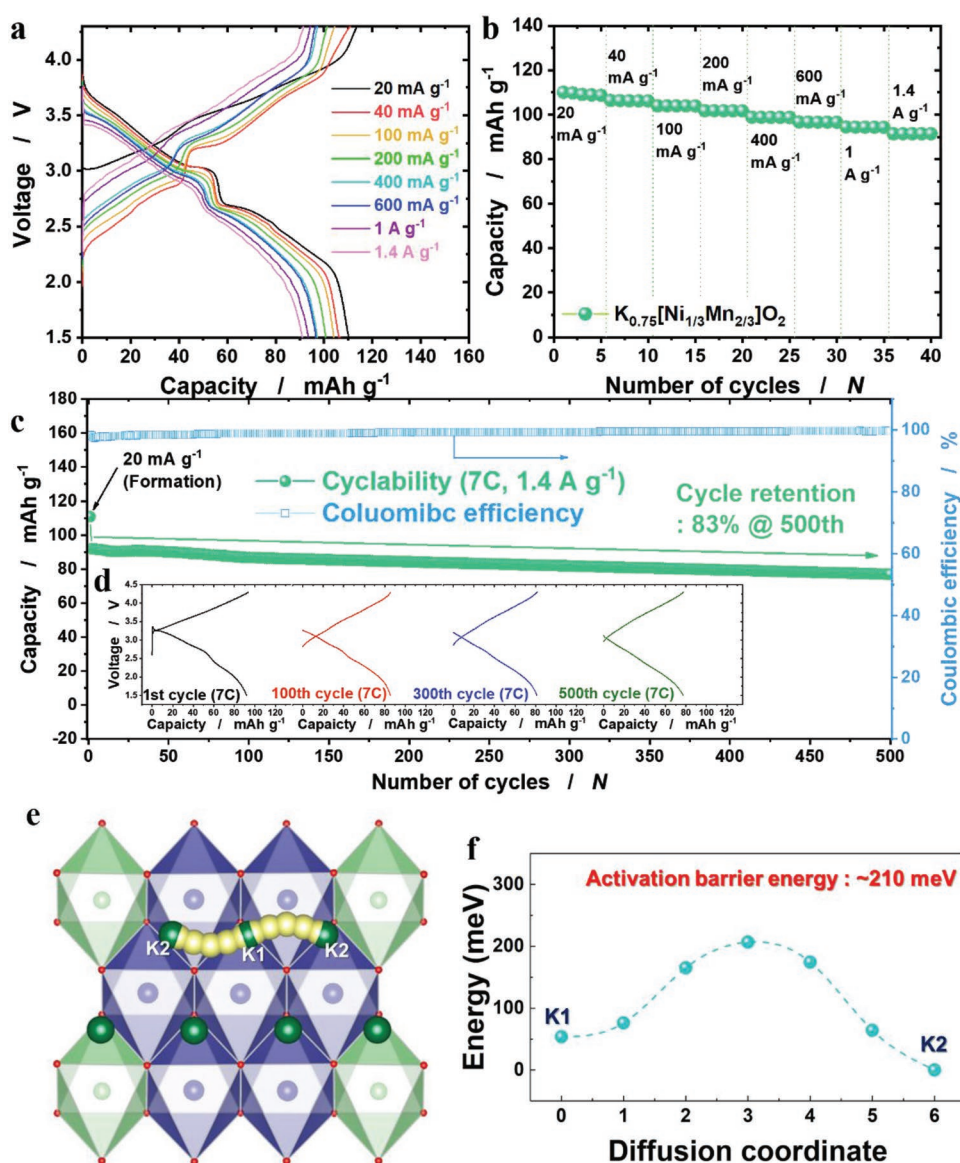


Figure 7. a) Charge–discharge curves at various currents from 20 to 1400 mA g^{-1} and b) the resulting rate capacities plot; c) cyclability for 500 cycles at 1400 mA g^{-1} ; d) selected charge-discharge voltage curves at 1st, 100th, 300th, and 500th at 1400 mA g^{-1} ; e) predicted K^+ diffusion motion in P2- $\text{K}_x[\text{Ni}_{1/3}\text{Mn}_{2/3}]\text{O}_2$ structure; and f) activation barrier energy for K^+ diffusion between K1 and K2 sites predicted using NEB method.

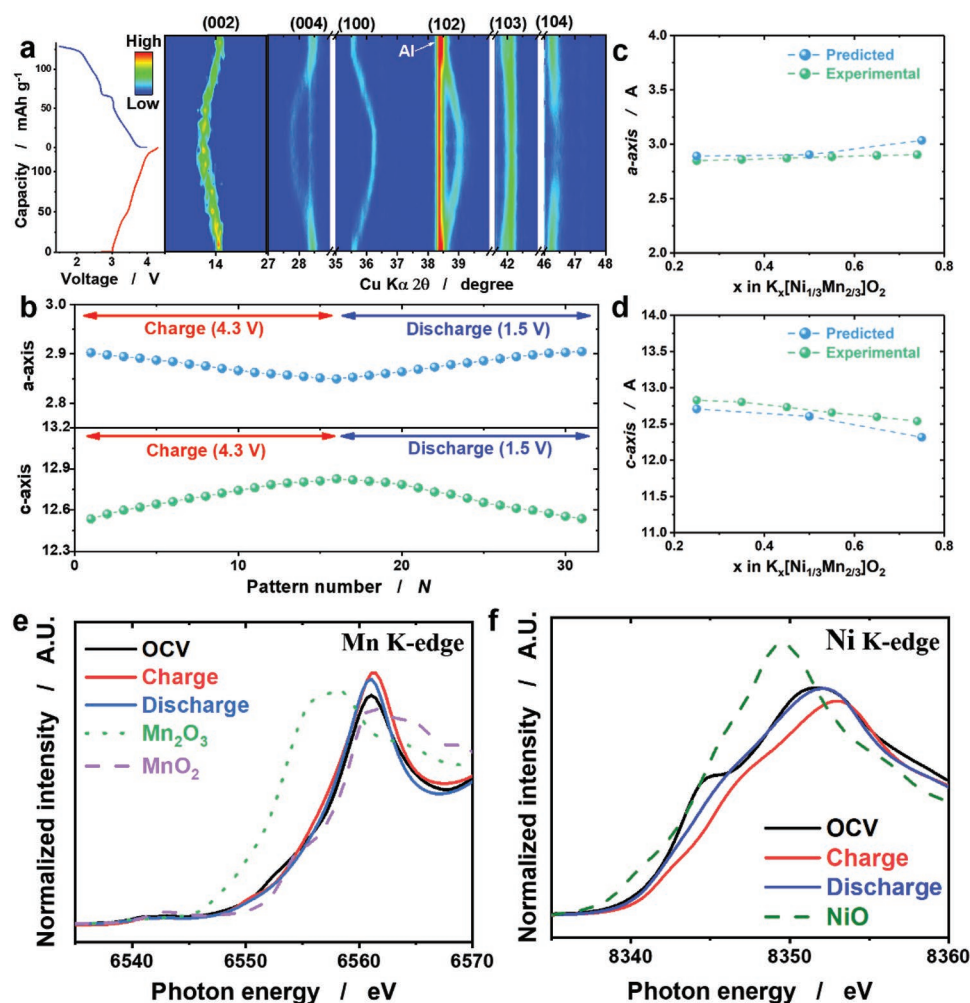


Figure 8. a) Operando-XRD result of P2- $K_{0.75}[Ni_{1/3}Mn_{2/3}]O_2$ electrode and b) the corresponding calculated lattice parameters for o-XRD pattern; c) comparison of a -axis and d) c -axis parameters of P2- $K_{0.75}[Ni_{1/3}Mn_{2/3}]O_2$ predicted from the first-principles calculations and experimentally obtained results from (b); e) XANES results for Mn K-edge and f) XANES results of Ni K-edge for P2- $K_{0.75}[Ni_{1/3}Mn_{2/3}]O_2$ electrodes: as-prepared, charged to 4.3 V, and discharged to 1.5 V.

acidity potassium can affect the fast ionic conductivity and, thereby, high capacity even at high rates.

To understand the structural evolution of the P2- $K_{0.75}[Ni_{1/3}Mn_{2/3}]O_2$ in K-cells, o-XRD and ex situ XANES analyses were performed during charge and discharge. Upon depotassiation (oxidation) to 4.3 V, the main (002) and (004) diffraction peaks of P2- $K_{0.75}[Ni_{1/3}Mn_{2/3}]O_2$ gradually moved toward lower angle, whereas the (100), (102), (103), and (104) peaks shifted toward higher angles (Figure 8a). This structural change behavior is consistent with the calculated lattice parameters; namely, the a -axis gradually decreased but the c -axis increased because of repulsive interaction between oxygen ions in the structure, caused by the extraction of K^+ from the structure (Figure 8b). No other phases were detected during the charge. During potassiation (reduction) to 1.5 V, the main peaks of P2- $K_{0.75}[Ni_{1/3}Mn_{2/3}]O_2$ reversibly returned to the original Bragg peak positions (Figure 8a), although K/vacancy ordering was observed in the discharge curve. The calculated lattice parameters were recovered to those of the fresh state

(Figure 8b). In addition, we compared the lattice parameters of P2- $K_{0.75}[Ni_{1/3}Mn_{2/3}]O_2$ with various K contents predicted by first-principles calculation with those verified by Rietveld refinement based on operando XRD patterns. As shown in Figure 8c,d, it was verified that the experimentally confirmed structural change of P2- $K_{0.75}[Ni_{1/3}Mn_{2/3}]O_2$ was consistent with the results of the first-principles calculation. This phase variation for de/potassiation demonstrates the occurrence of a simple single-phase reaction. The ex situ XANES data in Figure 8e shows the activity of the $Ni^{4+/2+}$ redox pair on oxidation and reduction. In contrast, the activity of Mn was not observed because there were no changes in the absorption spectra for charge and discharge (Figure 8f).

This redox reaction of P2- $K_{0.75}[Ni_{1/3}Mn_{2/3}]O_2$ during K^+ de/intercalation was also confirmed through first-principles calculation. As presented in Figure 9a,b, we arranged the integrated spin moments of Ni and Mn ions in P2- $K_{0.75}[Ni_{1/3}Mn_{2/3}]O_2$, P2- $K_{0.5}[Ni_{1/3}Mn_{2/3}]O_2$, and P2- $K_{0.25}[Ni_{1/3}Mn_{2/3}]O_2$. It was predicted that during K^+ deintercalation from P2- $K_{0.75}[Ni_{1/3}Mn_{2/3}]O_2$, the

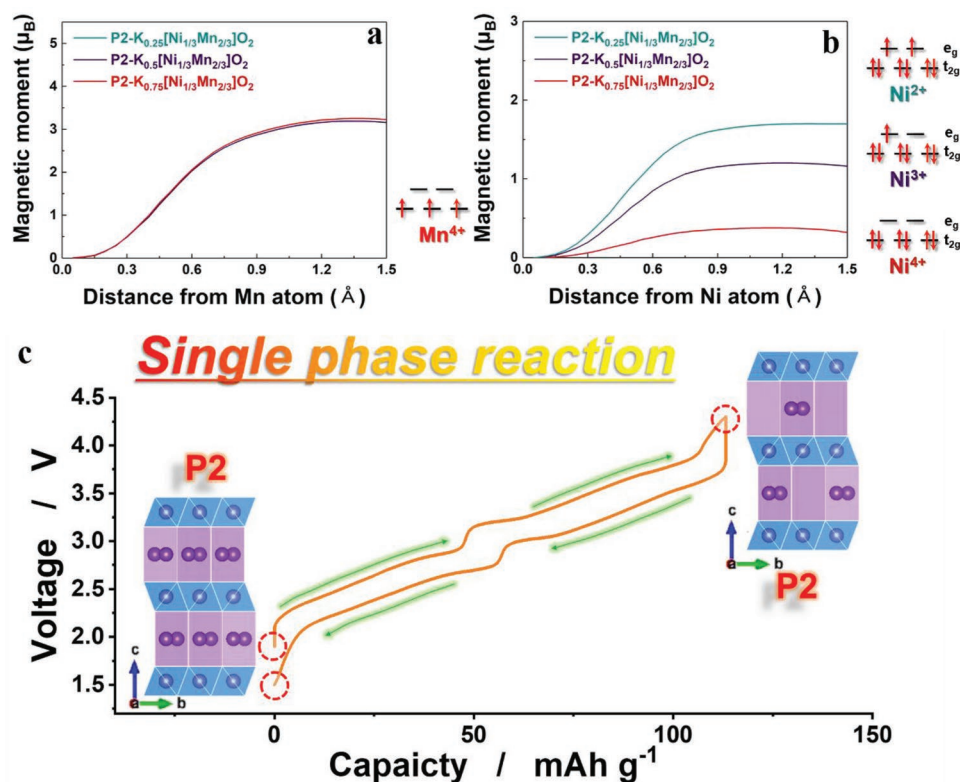


Figure 9. Spin integrations of a) Mn and b) Ni ions in P2-K_{0.75}[Ni_{1/3}Mn_{2/3}]O₂. c) Associated electrochemical reaction process of P2-K_{0.75}[Ni_{1/3}Mn_{2/3}]O₂ in K cells.

total electron spin of the Ni ions in the structure was monotonically increased from zero to two; however, that of the Mn ions maintained at three. These results imply that P2-K_{0.75}[Ni_{1/3}Mn_{2/3}]O₂ undergoes via Ni²⁺/Ni⁴⁺ redox reaction while Mn⁴⁺ was inactive during K⁺ de/intercalation in the operation range.

This finding suggests that Mn⁴⁺ in the structure plays a significant role in supporting the crystal structure. The P2-O2 phase transition is known as the result in a volume change of ≈23% in P2-Na_{2/3}[Ni_{1/3}Mn_{2/3}]O₂,^[44] which accelerates drastic capacity fading. The present P2-K_{0.75}[Ni_{1/3}Mn_{2/3}]O₂ experiences a single-phase reaction maintaining the P2 phase, such that the corresponding volume change was only ≈3.1%. Although NiO₆ octahedra can be affected by the variation of oxidation state of Ni²⁺ (0.69 Å) to Ni⁴⁺ (0.48 Å) during de/potassiation, Mn⁴⁺, which is 2/3 of the oxide matrix, is inactive but supports the structure. The single-phase reaction activated by the Ni^{4+/2+} redox pair and structural stability provided by the presence of Mn⁴⁺ are plausible reasons for the excellent long-term electrochemical performance even at high rates. The related electrochemical mechanism for P2-K_{0.75}[Ni_{1/3}Mn_{2/3}]O₂ is summarized in Figure 9c.

The post-cycled electrode tested at 20 mA g⁻¹ was monitored using XRD and HR-TEM. The Rietveld refinement of XRD data for the K_{0.75}[Ni_{1/3}Mn_{2/3}]O₂ electrode after 300 cycles demonstrates that the original layered structure was not much altered even after extensive cycles (Figure 10a and Table S5, Supporting Information). The post-cycled K_{0.75}[Ni_{1/3}Mn_{2/3}]O₂ particle still retained a similar shape as that of the as-prepared

K_{0.75}[Ni_{1/3}Mn_{2/3}]O₂ (Figure 10b), and the corresponding SAED patterns along the [00-1] zone axis were consistent with that of the as-prepared K_{0.75}[Ni_{1/3}Mn_{2/3}]O₂ hexagonal layered structure (Figure 10c). The elemental mappings clearly indicate that the K, Ni, and Mn elements were still present in the particle, without Na element (Figure 10d). The calculated lattice parameters were maintained, Δ*a* = 0.003 Å and Δ*c* = 0.008 Å, after the long-term cycling test, compared with the as-prepared P2-K_{0.75}[Ni_{1/3}Mn_{2/3}]O₂. Figure 11 and Figure S4 (Supporting Information) compared the electrode performance of high/low rate for several layered compounds.^[16,19,21,24,27,45,49–52] This result confirms the structural stability provided by Mn⁴⁺ in the oxide matrix of P2-K_{0.75}[Ni_{1/3}Mn_{2/3}]O₂. The above experimental and theoretical aspects suggest the feasibility of the present P2-K_{0.75}[Ni_{1/3}Mn_{2/3}]O₂ as a long-term sustainable cathode material for KIBs. Scale-up production of P2-K_x[Ni_{1/3}Mn_{2/3}]O₂ material is also an important concern to further develop these kinds of electrode materials for KIBs, and it is thought that chemical ionic exchange between Na⁺ and K⁺ would be a possible approach as we have witnessed the successful results from NaMnO₂ to LiMnO₂^[53] and from Na₂Ti₃O₇ to Li₄Ti₅O₁₂.^[54]

3. Conclusion

We propose layered P2-K_{0.75}[Ni_{1/3}Mn_{2/3}]O₂ as a novel high rate cathode material for KIBs. The electrode delivers a

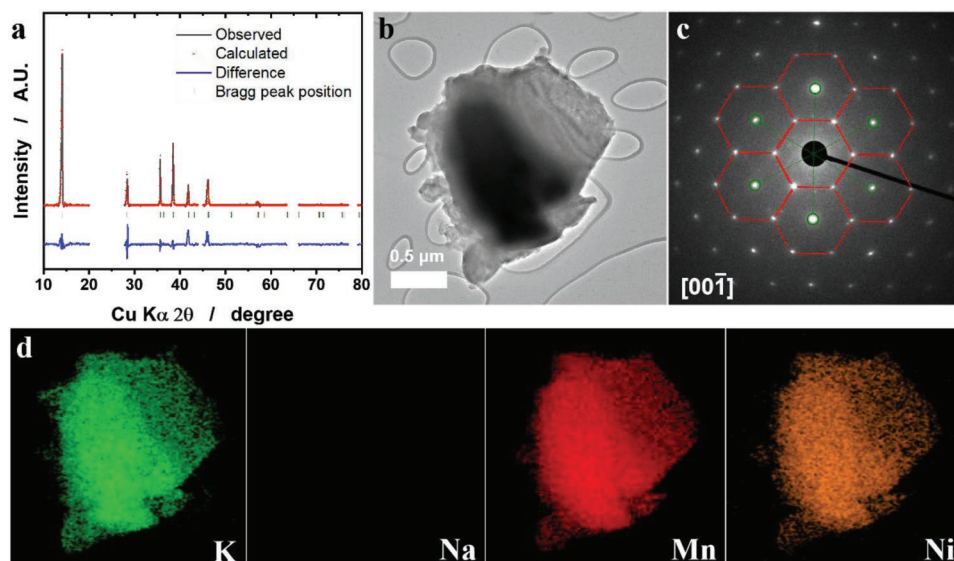


Figure 10. a) Rietveld refinement of XRD data for the post-cycled P2- $K_{0.75}[Ni_{1/3}Mn_{2/3}]O_2$ after 300 cycles at 20 mA g^{-1} ; b) TEM image of the post-cycled P2- $K_{0.75}[Ni_{1/3}Mn_{2/3}]O_2$ and c) the resulting SAED pattern and d) EDS mapping images.

discharge capacity of 110 mAh g^{-1} (20 mA g^{-1}) with a capacity retention of 86% after 300 cycles. Furthermore, the proposed $K_{0.75}[Ni_{1/3}Mn_{2/3}]O_2$ exhibited an unexpectedly high discharge capacity of about 91 mAh g^{-1} at 1400 mA g^{-1} , retaining 83% of capacity over 500 cycles. Combined studies using operando synchrotron X-ray diffraction, ex situ X-ray absorption near-edge structure spectroscopy confirmed that $K_{0.75}[Ni_{1/3}Mn_{2/3}]O_2$ undergoes via a single-phase reaction accompanied by the $Ni^{4+/2+}$ redox couple. According to experimental and theoretical results, it is suggested that the remarkable electrode performances at high-rate is attributed to the single-phase reaction with the $Ni^{4+/2+}$ redox couple. Furthermore, we confirm the experimental results and reaction mechanism on P2- $K_{0.75}[Ni_{1/3}Mn_{2/3}]O_2$ using a theoretical approach based on first-principles calculation. Our findings demonstrate the potential of layered structure $K_{0.75}[Ni_{1/3}Mn_{2/3}]O_2$ as a new candidate cathode material for KIBs.

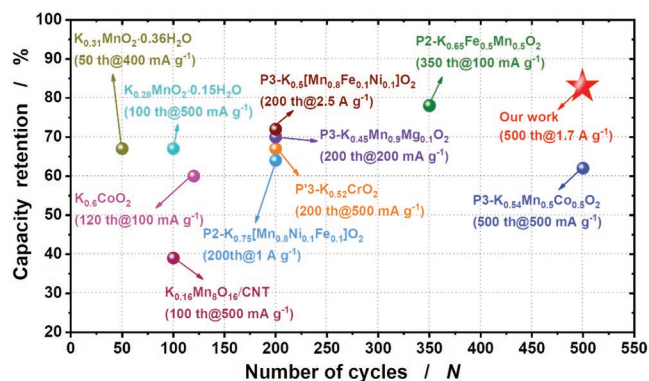


Figure 11. Comparison of high rate cycling performances for several layered compounds (there is comparison of low rate cycling performances for sample compound in Figure S4 in the Supporting Information).

Supporting Information

Supporting Information is available from the Wiley Online Library or from the author.

Acknowledgements

This research was supported by the Basic Science Research Program through the National Research Foundation of Korea (NRF), funded by the Ministry of Education, Science, and Technology of Korea (NRF-2017R1A2A2A05069634, NRF-2015M3D1A1069713, and NRF-2019H1D8A2106002).

Conflict of Interest

The authors declare no conflict of interest.

Keywords

battery, cathode, first-principle calculation, layered structure, potassium

Received: November 2, 2019
Revised: December 4, 2019
Published online: January 12, 2020

- [1] J. H. Jo, C. H. Jo, H. Yashiro, S. J. Kim, S. T. Myung, *J. Power Sources* **2016**, 313, 1.
- [2] M. Winter, J. O. Besenhard, M. E. Spahr, P. Novak, *ChemInform* **2010**, 29, 725.
- [3] B. Scrosati, J. Garche, *J. Power Sources* **2010**, 195, 2419.
- [4] B. Dunn, H. Kamath, J. M. Tarascon, *Science* **2011**, 334, 928.
- [5] L. Xue, Y. Li, H. Gao, W. Zhou, X. Lü, W. Kaveevivitchai, A. Manthiram, J. B. Goodenough, *J. Am. Chem. Soc.* **2017**, 139, 2164.

- [6] K. Beltrop, S. Beuker, A. Heckmann, M. Winter, T. Placke, *Energy Environ. Sci.* **2017**, *10*, 2090.
- [7] Y. Liu, Z. Tai, Q. Zhang, H. Wang, W. K. Pang, H. K. Liu, K. Konstantinov, Z. Guo, *Nano Energy* **2017**, *35*, 36.
- [8] C. D. Wessells, S. V. Peddada, R. A. Huggins, Y. Cui, *Nano Lett.* **2011**, *11*, 5421.
- [9] A. Eftekhari, Z. Jian, X. Ji, *ACS Appl. Mater. Interfaces* **2017**, *9*, 4404.
- [10] H. Kim, J. C. Kim, M. Bianchini, D. H. Seo, J. Rodriguez-Garcia, G. Ceder, *Adv. Energy Mater.* **2018**, *8*, 1702384.
- [11] J. Y. Hwang, S. T. Myung, Y. K. Sun, *Adv. Funct. Mater.* **2018**, *28*, 1802938.
- [12] A. Eftekhari, *ACS Sustainable Chem. Eng.* **2019**, *7*, 3684.
- [13] A. Eftekhari, *ACS Sustainable Chem. Eng.* **2019**, *7*, 5602.
- [14] W. Zhang, Y. Liu, Z. Guo, *Sci. Adv.* **2019**, *5*, 1.
- [15] Y. Hironaka, K. Kubota, S. Komaba, *Chem. Commun.* **2017**, *53*, 3693.
- [16] T. Deng, X. Fan, J. Chen, L. Chen, C. Luo, X. Zhou, J. Yang, S. Zheng, C. Wang, *Adv. Funct. Mater.* **2018**, *28*, 1.
- [17] T. Masese, K. Yoshii, M. Kato, K. Kubota, Z. D. Huang, H. Senoh, M. Shikano, *Chem. Commun.* **2019**, *55*, 985.
- [18] T. Deng, X. Fan, C. Luo, J. Chen, L. Chen, S. Hou, N. Eidson, X. Zhou, C. Wang, *Nano Lett.* **2018**, *18*, 1522.
- [19] J.-Y. Hwang, J. Kim, T.-Y. Yu, H.-G. Jung, J. Kim, K.-H. Kim, Y.-K. Sun, *J. Mater. Chem. A* **2019**, *7*, 21362.
- [20] C. I. Liu, S. h. Luo, H. b. Huang, Y. c. Zhai, Z. w. Wang, *Chem. Eng. J.* **2019**, *356*, 53.
- [21] J.-U. Choi, J. Kim, J. H. Jo, H. J. Kim, Y. H. Jung, D.-C. Ahn, Y. K. Sun, S. T. Myung, *Energy Storage Mater.* **2019**, <https://doi.org/10.1016/j.ensm.2019.09.015>.
- [22] J. Y. Hwang, J. Kim, T. Y. Yu, S. T. Myung, Y. K. Sun, *Energy Environ. Sci.* **2018**, *11*, 2821.
- [23] H. Kim, D.-H. Seo, J. C. Kim, S.-H. Bo, L. Liu, T. Shi, G. Ceder, *Adv. Mater.* **2017**, *29*, 1702480.
- [24] J. U. Choi, J. Kim, J. Y. Hwang, J. H. Jo, Y. K. Sun, S. T. Myung, *Nano Energy* **2019**, *61*, 284.
- [25] X. Wang, P. Hu, C. Niu, J. Meng, X. Xu, X. Wei, C. Tang, W. Luo, L. Zhou, Q. An, L. Mai, *Nano Energy* **2017**, *35*, 71.
- [26] X. Wang, X. Xu, C. Niu, J. Meng, M. Huang, X. Liu, Z. Liu, L. Mai, *Nano Lett.* **2017**, *17*, 544.
- [27] C. I. Liu, S. h. Luo, H. b. Huang, Y. c. Zhai, Z. w. Wang, *ChemElectroChem* **2019**, *6*, 2308.
- [28] S. Wang, T. Sun, S. Yuan, Y. H. Zhu, X. B. Zhang, J. M. Yan, Q. Jiang, *Mater. Horiz.* **2017**, *4*, 1122.
- [29] S. Wang, Y. H. Zhu, J. M. Yan, X. B. Zhang, *J. Mater. Chem. A* **2018**, *6*, 13075.
- [30] C. Liu, S. Luo, H. Huang, Z. Wang, A. Hao, Y. Zhai, Z. Wang, *Electrochem. Commun.* **2017**, *82*, 150.
- [31] C. Vaalma, G. A. Giffin, D. Buchholz, S. Passerini, *J. Electrochem. Soc.* **2016**, *163*, A1295.
- [32] J. Han, G. N. Li, F. Liu, M. Wang, Y. Zhang, L. Hu, C. Dai, M. Xu, *Chem. Commun.* **2017**, *53*, 1805.
- [33] W. B. Park, S. C. Han, C. Park, S. U. Hong, U. Han, S. P. Singh, Y. H. Jung, D. Ahn, K. S. Sohn, M. Pyo, *Adv. Energy Mater.* **2018**, *8*, 1703099.
- [34] J. H. Jo, J.-Y. Hwang, J. U. Choi, H. J. Kim, Y.-K. Sun, S.-T. Myung, *J. Power Sources* **2019**, *432*, 24.
- [35] A. Eftekhari, *J. Power Sources* **2004**, *126*, 221.
- [36] C. D. Wessells, R. A. Huggins, Y. Cui, *Nat. Commun.* **2011**, *2*, 550.
- [37] J. Wang, L. Zhang, L. Yu, Z. Jiao, H. Xie, X. W. Lou, X. Wei Sun, *Nat. Commun.* **2014**, *5*, 4921.
- [38] X. Wu, Z. Jian, Z. Li, X. Ji, *Electrochem. Commun.* **2017**, *77*, 54.
- [39] X. Bie, K. Kubota, T. Hosaka, K. Chihara, S. Komaba, *J. Mater. Chem. A* **2017**, *5*, 4325.
- [40] P. Sharma, D. Damien, K. Nagarajan, M. M. Shaijumon, M. Hariharan, *J. Phys. Chem. Lett.* **2013**, *4*, 3192.
- [41] Z. Jian, Y. Liang, I. A. R. Pérez, Y. Yao, X. Ji, *Electrochem. Commun.* **2016**, *71*, 5.
- [42] K. Sada, B. Senthilkumar, P. Barpanda, *Chem. Commun.* **2017**, *53*, 8588.
- [43] J. H. Jo, J. U. Choi, A. Konarov, H. Yashiro, S. Yuan, L. Shi, Y. K. Sun, S. T. Myung, *Adv. Funct. Mater.* **2018**, *28*, 1705968.
- [44] C. H. Jo, J. H. Jo, H. Yashiro, S. J. Kim, Y. K. Sun, S. T. Myung, *Adv. Energy Mater.* **2018**, *8*, 1702942.
- [45] N. Naveen, W. B. Park, S. C. Han, S. P. Singh, Y. H. Jung, D. Ahn, K. S. Sohn, M. Pyo, *Chem. Mater.* **2018**, *30*, 2049.
- [46] K. Kubota, I. Ikeuchi, T. Nakayama, C. Takei, N. Yabuuchi, H. Shiiba, M. Nakayama, S. Komaba, *J. Phys. Chem. C* **2015**, *119*, 166.
- [47] G. K. P. Dathar, D. Sheppard, K. J. Stevenson, G. Henkelman, *Chem. Mater.* **2011**, *23*, 4032.
- [48] K. Hoang, M. D. Johannes, *J. Mater. Chem. A* **2014**, *2*, 5224.
- [49] H. Kim, J. C. Kim, S.-H. Bo, T. Shi, D.-H. Kwon, G. Ceder, *Adv. Energy Mater.* **2017**, *7*, 1700098.
- [50] J. H. Jo, J. Hwang, J. Choi, Y. Sun, S. Myung, *ACS Appl. Mater. Interfaces* **2019**, *11*, 43312.
- [51] A. Gao, M. Li, N. Guo, D. Qiu, Y. Li, S. Wang, X. Lu, F. Wang, R. Yang, *Adv. Energy Mater.* **2019**, *9*, 1.
- [52] S. Chong, Y. Wu, C. Liu, Y. Chen, S. Guo, Y. Liu, G. Cao, *Nano Energy* **2018**, *54*, 106.
- [53] A. R. Armstrong, P. G. Bruce, *Nature* **1996**, *381*, 499.
- [54] K. T. Kim, C. Y. Yu, C. S. Yoon, S. J. Kim, Y. K. Sun, S. T. Myung, *Nano Energy* **2015**, *12*, 725.